Modeling of uncertainties in long fiber reinforced thermoplastics

Jörg Hohe*, Carla Beckmann, Hanna Paul

Fraunhofer-Institut für Werkstoffmechanik IWM
Wöhlerstr. 11, 79108 Freiburg, Germany

May 27, 2014

Abstract

The present study is concerned with a numerical scheme for the prediction of the uncertainty of the effective elastic properties of long fiber reinforced composites with thermoplastic matrix (LFT) produced by standard injection or press molding technologies based on the uncertainty of the microstructural geometry and topology. The scheme is based on a simple analysis of the single-fiber problem using the rules of mixture. The transition to the multi-fiber problem with different fiber orientations is made by the formulation of an ensemble average with defined probability distributions for the fiber angles. In the result, the standard deviations of the local fiber angles together with the local fiber content are treated as stochastic variables. The corresponding probability distributions for the effective elastic constants are determined in a numerically efficient manner by a discretization of the space of the random variables and the analysis of predefined cases within this space.

Key words: A: Polymer matrix composites, E: Mechanical properties, F: Microstructure.

1 Introduction

Long fiber reinforced composite materials with thermoplastic matrix are a new class of material combining the advantages of short fiber reinforced plastics and infinite fiber reinforced materials. Due to the limited fiber length, they can be processed using standard processing technologies for thermoplastic materials such as injection or press molding. On the other hand, compared to standard short fiber reinforced materials, the increased fiber length results in superior properties especially in terms of the effective strength. Major disadvantages of long fiber reinforced materials are their process-dependent microstructures (see Fig. 1) leading to spatial variations in the fiber mean orientation and thus the local effective properties as pointed out, among others, by Skourlis et al. [1] or Teixeira et al. [2] or Seelig et al. [3]. The latter study reports an example of a moulded component consisting of glass fiber reinforced polypropylene which exhibits strong effects of the local fiber distribution. Their simulation results with and without consideration reveal that without consideration of the actual local fiber orientation, no useful results can be obtained.

In addition to the local variation of the effective material properties due to the moulding process, the disordered irregular microstructure of LFT materials (see e.g. tomographic investigations reported by Garesci and Fliegener [4]) causes a distinct non-negligible uncertainty in their local effective properties even for known means of the fiber orientation. This uncertainty is a physical uncertainty deriving from the fact that the orientation of individual fibers cannot be predicted in a deterministically exact manner (Thomason [5]). Hence, the local fiber orientation at any specific position is subject to a variability causing an uncertainty in the local effective material properties at the respective spatial point. Consequently, experimental data for the effective material parameters is usually subject to a distinct scatter as e.g. reported by Seelig et al. [3] for specimens taken from the flow range (see Figure 2).

The numerical prediction of the effective properties for short and long fiber reinforced materials accounting for uncertainty effects caused by their disordered microstructure is a challenging task. Appropriate models have to account for the possibility of multiple fiber orientations occurring in limited spatial ranges. For this purpose,

*Corresponding author. Tel: +49-761-5142-340, Fax: +49-761-5142-510, E-mail: joerg.hohe@iwm.fraunhofer.de

a number of advanced material models and simulation strategies have been developed in literature. Taya and Chou [6] have provided a model for the elastic moduli for short fiber composites with random fiber orientation using an ellipsoidal fiber model based on Eshelby's tensor accounting for different fiber orientations based on assumed fiber orientations. In a similar manner, Nguyen and Khaleel [7] used a Mori-Tanaka analysis in conjunction with an averaging procedure to account for different possible fiber orientations. Garesci and Fliegener [4] have provided an analytical model for LFT materials with, based on the Halpin-Tsai fiber model to account for the non-even fiber orientation distribution. An experimental characterization of short fiber composites together with a simplified analytical model based thereon, accounting for the fiber orientation distribution has been provided by Dunn et al. [8]. In a similar manner, Fu and Lauke [9] have considered the probability functions for fiber length and orientation and developed simplified formulae for average fiber stress and strength.

Although the microstructural disorder is accounted for in terms of probability distributions for fiber orientation and length, all previous models are still of the deterministic type since they provide deterministic values for the effective material properties in terms of averages. On the other hand, among others, Bijsterbosch and Gaymans [10] have shown that distinct spatial variabilities in the local fiber orientation distributions may develop during the manufacture of long glass fiber reinforced polyamide (PA) 6 materials using injection molding. As a result, a distinct local variability in local fiber orientation distribution and – as a consequence – a distinct variability in local failure strength and strain as well as the local impact toughness is obtained. In a more recent contribution, Phelps et al. [11] have shown that the attrition of fibers during the molding process causes a distinct variability of fiber length distribution of the final product even for initially constant fiber length due to breakages. Hence, a probabilistic analysis rather than a classical deterministic approach is necessary for an appropriate prediction of the material response of short and long fiber reinforced materials.

Comprehensive reviews on the application of stochastic approaches to the modelling of fiber reinforced composites as well as the mentioned and other effects causing uncertainties in the effective material behaviour of fiber reinforced polymeric materials have been provided by Sriramula and Chryssanthopoulos [12] or, recently, by Mesogitis et al. [13]. Although the necessity for probabilistic approaches, only few studies providing such models for short and long fiber composites are available in literature. The variability in the elastic response of short fiber composites has been analyzed by Lusti et al. [14] considering a multi-fiber representative volume element in conjunction with a probabilistic evaluation. The prediction of the elastic constants of – although non-infiltrated – networks of long fibers has been considered by Lee and Jasiuk [15] using a probabilistic numerical approach based on a substructure technique for a large-scale representative volume element. An analysis of a similar problem has been provided by Dirrenberger et al. [16] using an alternative analysis technique consisting of the multiple analysis of smaller testing volume elements in conjunction with a stochastic evaluation. Rahman and Chakraborty [17] have provided a stochastic analysis of particle and short fiber composite using a Mori-Tanaka estimate in conjunction with a Karhunen-Loève expansion of the results to be used as input parameters for a macroscopic elasticity model such as e.g. the model provided by Soize [18].

Aim of the present study is the determination of a simplified analytical scheme for prediction of the uncertainty in the effective elastic properties of structures and components consisting of long fiber reinforced thermoplastic materials. The scheme is based on a micromechanical consideration of the single fiber problem using the standard rules of mixture. Using the local fiber orientation distributions, the elastic properties of the multi-fiber material are obtained as an ensemble average. The material model allows the prediction of local elastic properties for the structure based on the local flow direction, fiber content and fiber orientation distribution.

Since both, the local fiber content and the local orientation distribution are uncertain due to process variabilities, the fiber volume fraction and the standard deviation of the fiber angle distribution are considered as random variables provided with probability density distributions. Adopting a numerical scheme proposed previously by the authors for the analysis of the effective properties of two- and three-dimensional solid foams (Hohe and Hardenacke [19]), a repeated determination of the elastic properties for predefined sets of the random variables is performed. Considering the individual probability of occurrence for the analyzed cases in the (hyper) space of the random variables, the probability distributions for the macroscopic elastic properties are obtained as a function of the microstructural uncertainties.

2 Numerical procedure

2.1 Material model

The material model proposed for the prediction of the effective elastic properties of long fiber reinforced thermoplastic materials is defined in three steps. In the first step, the case of a single fiber oriented arbitrarily in space

is considered. In the second step, a solution for the multi-fiber problem is derived, based on the solution for the single-fiber problem. In the third step, a probabilistic enhancement of the determinstic approach defined in the first two steps is defined.

For the analysis of the single-fiber problem, a local microscopic Cartesian coordinate system x_i' according to Fig. 3 is introduced. In the microscopic system, the x_1'-direction as usual coincides with the fiber direction whereas the x_2'- and x_3'-axes are oriented normally to the fiber direction. The microscopic fiber coordinate system is obtained from the macroscopic Cartesian system x_i by a rotation with respect to the x_3-axis by an angle φ. The macroscopic system x_i is oriented such that the x_1-x_2-plane coincides with the reference surface of the thin-walled LFT-structure with the x_1-direction as the flow (or otherwise preferred) direction of the manufacturing process. The possible misorientation of the fibers with respect to the reference surface of the thin-walled structure (i.e. an orientation out of the x_1-x_2-plane) is neglected since the average fiber length for LFT materials with maximum lengths in the range of $25\,\mathrm{mm}$ up to $50\,\mathrm{mm}$ is in the same order of magnitude for typical wall thicknesses and beyond. Notice that due to possible curvatures of the structure and process-dependent local changes of the flow direction (see Fig. 1), the macroscopic system x_i also has a local character.

In the analysis of the single-fiber problem, it is assumed that the fiber length – although finite – is large compared to the fiber diameter. The fibers may be curved, however, it is assumed that the curvature radii are large compared to the fiber diameter. For standard LFT materials, both conditions are usually satisfied. In this case, the effective elastic response on the single fiber level can be described by

$$\begin{pmatrix} \varepsilon_{11}' \\ \varepsilon_{22}' \\ \varepsilon_{33}' \\ 2\varepsilon_{23}' \\ 2\varepsilon_{13}' \\ 2\varepsilon_{12}' \end{pmatrix} = \begin{pmatrix} 1/E_1' & -\nu_{21}'/E_2' & -\nu_{31}'/E_3' & 0 & 0 & 0 \\ & 1/E_2' & -\nu_{32}'/E_3' & 0 & 0 & 0 \\ & & 1/E_3' & 0 & 0 & 0 \\ & & & 1/G_{23}' & 0 & 0 \\ & & & & 1/G_{13}' & 0 \\ \text{(sym.)} & & & & & 1/G_{12}' \end{pmatrix} \begin{pmatrix} \sigma_{11}' \\ \sigma_{22}' \\ \sigma_{33}' \\ \sigma_{23}' \\ \sigma_{13}' \\ \sigma_{12}' \end{pmatrix} \tag{1}$$

where the effective elasticity constants are approximated by the rules of mixture

$$\begin{aligned} E_1' &= \rho^{\mathrm{f}} E^{\mathrm{f}} + (1-\rho^{\mathrm{f}}) E^{\mathrm{m}} \quad , \quad E_2' = \frac{E^{\mathrm{f}} E^{\mathrm{m}}}{\rho^{\mathrm{f}} E^{\mathrm{m}} + (1-\rho^{\mathrm{f}}) E^{\mathrm{f}}} \quad , \quad E_3' = \frac{E^{\mathrm{f}} E^{\mathrm{m}}}{\rho^{\mathrm{f}} E^{\mathrm{m}} + (1-\rho^{\mathrm{f}}) E^{\mathrm{f}}} \\ \nu_{23}' &= \left(\rho^{\mathrm{f}} \nu^{\mathrm{f}} + (1-\rho^{\mathrm{f}}) \nu^{\mathrm{m}}\right) \quad , \quad \nu_{13}' = \left(\rho^{\mathrm{f}} \nu^{\mathrm{f}} + (1-\rho^{\mathrm{f}}) \nu^{\mathrm{m}}\right) \quad , \quad \nu_{12}' = \left(\rho^{\mathrm{f}} \nu^{\mathrm{f}} + (1-\rho^{\mathrm{f}}) \nu^{\mathrm{m}}\right) \\ \nu_{32}' &= \frac{E_3'}{E_2'} \nu_{23}' \quad , \quad \nu_{31}' = \frac{E_3'}{E_1'} \nu_{13}' \quad , \quad \nu_{21}' = \frac{E_2'}{E_1'} \nu_{12}' \\ G_{23}' &= \frac{E_2'}{2(1+\nu_{23}')} \quad , \quad G_{13}' = \frac{G^{\mathrm{f}} G^{\mathrm{m}}}{\rho^{\mathrm{f}} G^{\mathrm{m}} + (1-\rho^{\mathrm{f}}) G^{\mathrm{f}}} \quad , \quad G_{12}' = \frac{G^{\mathrm{f}} G^{\mathrm{m}}}{\rho^{\mathrm{f}} G^{\mathrm{m}} + (1-\rho^{\mathrm{f}}) G^{\mathrm{f}}} \end{aligned} \tag{2}$$

with the elastic constants E^{m}, ν^{m} and G^{m} of the matrix material, the constants E^{f}, ν^{f} and G^{f} of the fiber material and the fiber volume fraction ρ^{f}. Using Eqns. (1) and (2) implies that the material for both, the fibers and the matrix is linear elastic and that both constituents are bonded with a "pefect" interface without any compliance or damage. Both assumptions are indeed approximations. Nevertheless, under regular service conditions, the material remains in the small strain limit so that both assumptions are satisfied to a reasonable extent.

For a transformation into the macroscopic system x_i, Eq. (1) is rewritten to the standard tensor form using the relation

$$\begin{pmatrix} \varepsilon_{11}' \\ \varepsilon_{22}' \\ \varepsilon_{33}' \\ 2\varepsilon_{23}' \\ 2\varepsilon_{13}' \\ 2\varepsilon_{12}' \end{pmatrix} = \begin{pmatrix} D_{1111}' & D_{1122}' & D_{1133}' & D_{1123}' & D_{1113}' & D_{1112}' \\ & D_{2222}' & D_{2233}' & D_{2223}' & D_{2213}' & D_{2212}' \\ & & D_{3333}' & D_{3323}' & D_{3313}' & D_{3312}' \\ & & & D_{2323}' & D_{2313}' & D_{2312}' \\ & & & & D_{1313}' & D_{1312}' \\ \text{(sym.)} & & & & & D_{1212}' \end{pmatrix} \begin{pmatrix} \sigma_{11}' \\ \sigma_{22}' \\ \sigma_{33}' \\ \sigma_{23}' \\ \sigma_{13}' \\ \sigma_{12}' \end{pmatrix} \tag{3}$$

of the components D_{ijkl}' of the fourth order compliance tensor with the components D_{ij}' of the second order compliance matrix in Eq. (1). Substituting the compliance components D_{ijkl}' into the transformation equation

$$D_{ijkl} = a_{im} a_{jn} a_{kp} a_{lq} D_{mnpq}' \tag{4}$$

with the rotation matrix

$$a_{ij} = \begin{pmatrix} \cos\varphi & -\sin\varphi & 0 \\ \sin\varphi & \cos\varphi & 0 \\ 0 & 0 & 1 \end{pmatrix} \tag{5}$$

then yields the effective compliance components D_{ijkl} for the single-fiber problem with respect to the macroscopic coordinate system x_i (see Fig. 3).

In a second step, the effective elastic compliances for the multi-fiber problem are derived. For this purpose, a representative volume element Ω^{RVE} according to Fig. 3 is considered. For thin-walled injection or press molded structures as considered here, consideration of a shell-like volume element rather than a true three-dimensional volume element is appropriate. The representative volume element contains multiple fibers with different orientations defined by a prescribed probability density distribution $f(\varphi)$. Its effective compliance properties are determined as the ensemble average

$$\bar{D}_{ijkl} = \mathcal{E}(D_{ijkl}) = \int_{\varphi=-\pi/2}^{\pi/2} D_{ijkl}(\varphi) f(\varphi)\, \mathrm{d}\varphi \tag{6}$$

of the effective elastic properties D_{ijkl} for the single fiber problem. In Eq. (6), $\mathcal{E}(D_{ijkl})$ denotes the expectation value of the effective compliance components D_{ijkl} in the case that their probability is defined by the probability density distribution $f(\varphi)$. The integration range is defined by the interval $[-\pi/2, \pi/2]$ rather than the usual range $[-\infty, \infty]$ due to the π-periodicity of the problem.

The probability density distribution $f(\varphi)$ for the fiber orientation is defined as a Gaussian series

$$f(\varphi, s^{\mathrm{f}}, \mu^{\mathrm{f}}) = \begin{cases} 0 & \text{for } \varphi < -\frac{\pi}{2} \\ \displaystyle\sum_{i=-\infty}^{\infty} \frac{1}{s^{\mathrm{f}}(2\pi)^{1/2}}\, e^{-\frac{1}{2}\frac{(\mu^{\mathrm{f}} - (\varphi + i\pi))^2}{(s^{\mathrm{f}})^2}} & \text{for } -\frac{\pi}{2} \le \varphi < \frac{\pi}{2} \\ 0 & \text{for } \varphi \ge \frac{\pi}{2} \end{cases} \tag{7}$$

where s^{f} and μ^{f} are the standard deviation and the mean of the underlying Gaussian probability distributions forming the members of the series expansion (7). However, due to the series type formulation, these parameters do not have this direct mathematical meaning but simply constitute additional material parameters defining the scatter band width and position for the fiber angles within the representative volume element Ω^{RVE}. In Eq. (7), the series expansion of the standard Gaussian distribution corrects the error due to the cutoff at $\varphi = -\pi/2$ and $\pi/2$, i.e. it ensures that

$$\int_{-\infty}^{\infty} f(\varphi)\, \mathrm{d}\varphi = 1 \tag{8}$$

as a necessary condition for any kind of probability density distribution. Furthermore, it results in a smooth curvature without any kink at $\varphi = -\pi/2$ and $\varphi = \pi/2$.

To illustrate the shape of the proposed probability density distribution, the function $f(\varphi)$ is plotted in Fig. 4 for a position parameter of $\mu^{\mathrm{f}} = 0$ and five different scatter band widths with different s^{f}. For $\varphi = \pi/2$, the case of a uniform probability density distribution and thus an equal probability for all fiber angles φ is obtained. This type of probability density distribution is found in the injection or press region of LFT structures as it has been observed e.g. in tomographic investigations reported by Garesci and Fliegener [4]. Decreasing s^{f} result in decreasing scatter band widths and thus describe the situation in the flow regions far from the press or injection regions with increasingly aligned fibers. A similar probability density distribution, however of a non-series type and thus with a non-smooth characteristic at $\varphi = \pm\pi/2$, has been poposed by Dunn et al. [8] in their experimental and numerical study the elastic constants of short fiber reinforced metal matrix composites.

2.2 Probabilistic analysis

The scheme for prediction of the effective elasticity constants for long fiber reinforced materials defined by Eqns. (1) to (7) still defines a deterministic model, since – so far – the seven material parameters E^{m}, ν^{m}, E^{f}, ν^{f}, ρ^{f}, s^{f} and μ^{f} are prescribed in a deterministically exact manner. Nevertheless, especially those effective material parameters defining the microstructure of the representative volume element Ω^{RVE} are, in general, uncertain due to uncertainties in the injection or press molding processes. Hence, the local fiber volume fraction ρ^{f} together with the scatter band width parameter s^{f} are considered as random variables with prescribed probability density distributions $f_\rho(\rho^{\mathrm{f}})$ and $f_s(s^{\mathrm{f}})$ respectively. The scatter band position parameter μ^{f} could be treated in the

same manner, however, by an appropriate choice of the macroscopic coordinate system x_i ensuring $\mu^{\mathrm{f}} = 0$, this parameter can be eliminated.

In the present analysis, both probability density distributions are assumed to be of the logarithmic normal type

$$\begin{aligned} f_\rho(\rho^{\mathrm{f}}) &= \frac{1}{\rho^{\mathrm{f}} s_\rho (2\pi)^{1/2}}\, e^{-\left(\frac{\ln \rho^{\mathrm{f}} - \mu_\rho}{2^{1/2} s_\rho}\right)^2} \\ f_{\mathrm{s}}(s^{\mathrm{f}}) &= \frac{1}{s^{\mathrm{f}} s_{\mathrm{s}} (2\pi)^{1/2}}\, e^{-\left(\frac{\ln s^{\mathrm{f}} - \mu_{\mathrm{s}}}{2^{1/2} s_{\mathrm{s}}}\right)^2} \end{aligned} \tag{9}$$

with the stochastic material parameters μ_ρ, s_ρ, μ_{s} and s_{s}. In Eqns. (9) the position parameters μ_ρ and μ_{s} determine the position of the probability distribution and thus the scatter band whereas the shape parameters s_ρ and s_{s} govern the spreading of the probability distribution and thus the width of the scatter band. These parameters are related to the expectation values and standard deviations by:

$$\begin{aligned} \mathcal{E}(\rho^{\mathrm{f}}) &= e^{\mu^\rho + \frac{(s^\rho)^2}{2}} \quad , \quad \mathcal{S}(\rho^{\mathrm{f}}) = \left(e^{2\mu^\rho + (s^\rho)^2} \left(e^{(s^\rho)^2} - 1 \right) \right)^{\frac{1}{2}} \\ \mathcal{E}(s^{\mathrm{f}}) &= e^{\mu^{\mathrm{s}} + \frac{(s^{\mathrm{s}})^2}{2}} \quad , \quad \mathcal{S}(s^{\mathrm{f}}) = \left(e^{2\mu^{\mathrm{s}} + (s^{\mathrm{s}})^2} \left(e^{(s^{\mathrm{s}})^2} - 1 \right) \right)^{\frac{1}{2}} \end{aligned} \tag{10}$$

Within the present study, the parameters μ_ρ, s_ρ, μ_{s} and s_{s} are determined such that the predefined expectation values $\mathcal{E}(\rho^{\mathrm{f}})$ and $\mathcal{E}(s^{\mathrm{f}})$ as well as the predefined standard deviations $\mathcal{S}(\rho^{\mathrm{f}})$ and $\mathcal{S}(s^{\mathrm{f}})$ of the random variables ρ^{f} and s^{f} are obtained. Notice that the logarithmic normal probability distributions (9) used here are just assumptions. If for any kind of material other types of probability distribution for the random variables such as Gaussian, Weibull, exponential or other types are more apropriate, the type of probability distribution can easily be exchanged in the ongoing derivation. Even experimentally measured distributions without any kind of continuous approximation can be used, if desired.

Using Eq. (9) with μ_ρ, s_ρ, μ_{s} and s_{s} according to Eq. (10) or any other type of probability distributions for the random variables, a prediction of the scatter and uncertainty to be expected in the effective elastic properties $\bar{D}_{ijkl}$ due to the uncertainty in the random variables ρ^{f} and s^{f} – defining the local microstructural geometry of the material – is possible. As it has been pointed out in previous studies on the uncertainty of the effective properties of solid foams (Hohe and Hardenacke [19], Beckmann and Hohe [20]), a direct Monte-Carlo analysis is numerically inefficient, due to the extremely large number of microstructural cases to be analyzed in order to obtain numerically stable results even in the upper and lower tails of the resulting probability distributions $\mathcal{F}(\bar{D}_{ijkl})$ for the effective elastic properties $\bar{D}_{ijkl}$.

To circumvent this problem, the discretising numerical scheme proposed by the authors for solid foams (Hohe and Hardenacke [19]) is adopted. For this purpose, the (hyper) space of the random variables ρ^{f} and s^{f} is discretized according to Figure 5. For each node $(s_i^{\mathrm{f}}, \rho_j^{\mathrm{f}})$ with $i = 1, \ldots, n$ and $j = 1, \ldots, m$ in the discretized space of the random variables, the corresponding value $\bar{E}_k(s_i^{\mathrm{f}}, \rho_j^{\mathrm{f}})$, $\bar{G}_{kl}(s_i^{\mathrm{f}}, \rho_j^{\mathrm{f}})$ or $\bar{\nu}_{kl}(s_i^{\mathrm{f}}, \rho_j^{\mathrm{f}})$ of the considered effective property is computed. The individual probability for occurrence of the parameter combination $(s_i^{\mathrm{f}}, \rho_j^{\mathrm{f}})$ is

$$\begin{aligned} \mathrm{d}\mathcal{F}(s_i^{\mathrm{f}}, \rho_j^{\mathrm{f}}) &= p(s_i^{\mathrm{f}}) p(\rho_i^{\mathrm{f}}) \\ &= \int_{s^{\mathrm{f}} = \frac{1}{2}(s_i^{\mathrm{f}} - s_{i-1}^{\mathrm{f}})}^{\frac{1}{2}(s_{i+1}^{\mathrm{f}} - s_i^{\mathrm{f}})} \int_{\rho^{\mathrm{f}} = \frac{1}{2}(\rho_i^{\mathrm{f}} - \rho_{i-1}^{\mathrm{f}})}^{\frac{1}{2}(\rho_{i+1}^{\mathrm{f}} - s_i^{\mathrm{f}})} f_{\mathrm{s}}(s^{\mathrm{f}}) f_\rho(\rho^{\mathrm{f}})\, \mathrm{d}s^{\mathrm{f}} \mathrm{d}\rho^{\mathrm{f}} \end{aligned} \tag{11}$$

where $f_\rho(\rho^{\mathrm{f}})$ and $f_{\mathrm{s}}(s^{\mathrm{f}})$ are the probability density distributions for the random variables s^{f} and ρ^{f} according to Eq. (9) or – in the discretized approximation using a numerical one-point Gauss integration scheme –

$$\Delta\mathcal{F}_{ij} = f_{\mathrm{s}}(s_i^{\mathrm{f}}) f_\rho(\rho_j^{\mathrm{f}}) \Delta s_i^{\mathrm{f}} \Delta \rho_j^{\mathrm{f}} \tag{12}$$

where

$$\begin{aligned} \Delta s_i^{\mathrm{f}} &= \frac{1}{2}\left(s_{i+1}^{\mathrm{f}} - s_{i-1}^{\mathrm{f}} \right) \\ \Delta \rho_j^{\mathrm{f}} &= \frac{1}{2}\left(\rho_{j+1}^{\mathrm{f}} - \rho_{j-1}^{\mathrm{f}} \right) \end{aligned} \tag{13}$$

are the edge lengths of the elements in the discretized space of the random variables.

After computation of the effective elastic properties $\bar{E}_k(s_i^{\mathrm{f}}, \rho_j^{\mathrm{f}})$, $\bar{G}_{kl}(s_i^{\mathrm{f}}, \rho_j^{\mathrm{f}})$ and $\bar{\nu}_{kl}(s_i^{\mathrm{f}}, \rho_j^{\mathrm{f}})$ at the nodes of the discretized space of the random variables s^{f} and ρ^{f} together with the corresponding individual probability densities $\Delta\mathcal{F}_{ij}$ for occurrence of the parameter combination $(s_i^{\mathrm{f}}, \rho_j^{\mathrm{f}})$ – and thus the occurrence of the respective effective elastic properties based on this combination – the data for the effective properties are re-arranged into ascending order. Subsequently, the cumulative probabilities

$$\begin{aligned}
\mathcal{F}\left(\bar{E}_k(s_{i'}^{\mathrm{f}}, \rho_{j'}^{\mathrm{f}})\right) &= \sum_{p'=1}^{i'} \sum_{q'=1}^{j'} \Delta\mathcal{F}_{i'j'} \\
\mathcal{F}\left(\bar{G}_{kl}(s_{i'}^{\mathrm{f}}, \rho_{j'}^{\mathrm{f}})\right) &= \sum_{p'=1}^{i'} \sum_{q'=1}^{j'} \Delta\mathcal{F}_{i'j'} \\
\mathcal{F}\left(\bar{\nu}_{kl}(s_{i'}^{\mathrm{f}}, \rho_{j'}^{\mathrm{f}})\right) &= \sum_{p'=1}^{i'} \sum_{q'=1}^{j'} \Delta\mathcal{F}_{i'j'}
\end{aligned} \tag{14}$$

that the effective elastic properties attain the values $\bar{E}_k$, $\bar{G}_{kl}$ or $\bar{\nu}_{kl}$, respectively, or less can be computed. In this context, the indices i' and j' refer to the re-arranged order of the data sets for the elastic properties into ascending order. Notice, that the re-ordering, in general, will be different for the different effective elastic constants $\bar{E}_k$, $\bar{G}_{kl}$ and $\bar{\nu}_{kl}$, respectively, since it depends on the values of the respective data.

3 Example

3.1 Material example

As an illustrative example, a glass fiber reinforced PA 6 material as it can be manufactured e.g. by press molding processes is considered. The glass fibers are assumed to be linear elastic with a Young's modulus of $E^{\mathrm{f}} = 75\,\mathrm{GPa}$ and a Poisson's ratio of $\nu^{\mathrm{f}} = 0.25$. The matrix material behaviour is also approximated by Hooke's law with a Young's modulus and a Poisson's ratio of $E^{\mathrm{m}} = 3\,\mathrm{GPa}$ and $\nu^{\mathrm{m}} = 0.35$, respectively. Although the material response of PA 6 becomes essentially nonlinear in the high strain range, the linear Hooke's law with the mentioned material data provides a reasonably good approximation in the small strain range which is the relevant range here due to the stiff fiber reinforcement in different spatial directions. A similar material, although with a polyamide 6.6 matrix, has been investigated experimentally by Thomason [21].

Prior to the stochastic consideration, the basic dependence of the effective material constants on the stochastic variables s^{f} and ρ^{f} is investigated. The results are presented in Fig. 6. In this context, the variability s^{f} of the fiber orientation distribution is varied over the entire possible range $s^{\mathrm{f}} = 0, \ldots, \pi/2$. A fiber orientation variability of $s^{\mathrm{f}} = 0$ defines a perfect alignment of the fibers, i.e. corresponds to the case of an unidirectionally infinite fiber reinforced composite. For $s^{\mathrm{f}} = \pi/2$, the case of a "perfect" disorder of the fibers with an even fiber orientation distribution (Fig. 4) is attained as an extreme case. The injection or press region of typical LFT materials is typically found in the range $s^{\mathrm{f}} = 3\pi/8, \ldots, \pi/2$ close to the right hand side of the plots in Fig. 6 since in the injection and press regions, no preferences for the fiber orientation are to be expected (e.g. Garesci and Fliegener [4]). In contrast, the flow range is typically situated in the range $s^{\mathrm{f}} = 0, \ldots, \pi/8$ towards the left hand side of the figures since for increasing flow distance, an increasing amount of fiber re-orientation will occur. However, the amounts of fiber orientation variability depend on the flow path and distance before solidification and thus may differ (Teixeira et al. [2]). For all cases considered in Fig. 6, five different fiber volume fractions in the range $\rho^{\mathrm{f}} = 0.1, \ldots, 0.3$ are considered. Typical fiber volume fractions for press or injection molded long fiber reinforced thermoplastics are in the range of $\rho^{\mathrm{f}} = 0.1$ to 0.15.

It is observed in Fig. 6 that the effective Young's modulus $\bar{E}_1^{\mathrm{LFT}}$ within the flow or preferred direction is close to the corresponding value E_1' for unidirectionally fiber reinforced composites. (Fig. 3). If an increasing disorder of the microstructure with increasing fiber orientation variabilities s^{f} occurs, a rapid decrease of the effective Young's modulus $\bar{E}_1^{\mathrm{LFT}}$ is observed, down to values as low as approximately 20% of the maximum possible stiffness, if the case of a "perfect" disorder is approached for $s^{\mathrm{f}} \to \pi/2$. At the same time, the effective Young's modulus $\bar{E}_2^{\mathrm{LFT}}$ perpendicular to the preferred or flow direction increases for increasing fiber orientation variabilities s^{f}. Nevertheless, the increase in the perpendicular stiffness $\bar{E}_2^{\mathrm{LFT}}$ is much less distinct than the contemporary decrease of the effective Young's modulus $\bar{E}_1^{\mathrm{LFT}}$ within the preferred direction. The transverse effective Young's modulus $\bar{E}_3^{\mathrm{LFT}}$ is not affected by variations in the fiber orientation variability s^{f} since in the considered thin shell limit, all fibers are assumed to be located within the x_1-x_2-surface with no variations.

As expected, increasing fiber volume fractions result in an increasing stiffness of the material with increasing effective elastic moduli $\bar{E}_i^{\mathrm{LFT}}$ in all spatial directions.

For the effective in-plane shear modulus $\bar{G}_{12}^{\mathrm{LFT}}$ a moderate increase is observed, if the fiber orientation variability s^{f} is increased from the extreme case of a unidirectionally fiber reinforced material at $s^{\mathrm{f}} = 0$. This increase is caused by the increasing amount of fibers orientated towards the $\pm\pi/2$-direction with the maximum tensile and compressive normal stresses in case of a pure shear load $\bar{\sigma}_{12}$ applied in the x_1-x_2-plane. The observed increase is restricted to small fiber orientation variabilities $s^{\mathrm{f}} < 3\pi/16$. For fiber orientation variabilities beyond $s^{\mathrm{f}} \approx \pi/4$, almost no effect of the fiber orientation variability s^{f} on the effective in-plane shear modulus $\bar{G}_{12}^{\mathrm{LFT}}$ is observed. For the two transverse effective shear moduli $\bar{G}_{23}^{\mathrm{LFT}}$ and $\bar{G}_{13}^{\mathrm{LFT}}$, nearly no effects of variations in the fiber orientation variability s^{f} are obtained. Both quantities are dominated by the shear properties of the matrix material with $G^{\mathrm{m}} = E^{\mathrm{m}}/(2(1+\nu^{\mathrm{m}}))$ which is increased only slightly by the glass fiber reinforcement oriented entirely within the x_1-x_2-plane.

The effective Poisson's ratios $\bar{\nu}_{32}^{\mathrm{LFT}}$ and $\bar{\nu}_{31}^{\mathrm{LFT}}$ transversal to x_1-x_2-plane as the reference plane of the structure as well as the effective Poisson's ratio $\bar{\nu}_{21}^{\mathrm{LFT}}$ within the reference surface are strongly affected by the effective elastic moduli of the material on the macroscopic level. Furthermore, they are not bounded by the corresponding microscopic elastic properties of the constituent materials as in the case of the effective Young's and shear moduli. As a consequence, stronger variations of all three effective Poisson's ratios are obtained compared to the effective Young's and shear moduli. The results on the dependence of the effective elastic properties of LFT materials on the microstructural constitutive parameters s^{f} and ρ^{f} reveal that by an appropriate design of the molding process, improved elastic properties of the final product can be attained.

3.2 Uncertainty effects

In contrast to the assumption of predefined, deterministic values for the local fiber orientation variability s^{f} and the local fiber volume fraction ρ^{f} in Sec. 3.1, both quantities are subject to uncertainties due to uncertainties in the non-consolidated material as well as uncertainties in the molding process (Teixeira et al. [2], Seelig et al. [3], Garesci and Fliegener [4]). Hence, a probabilistic treatment of the elastic properties rather than the previous deterministic treatment is required.

For this purpose, the probabilistic methods defined in Sec. 2.2 are applied to the model material described in Sec. 3.1. As a reference case for the probabilistic analyses, the expectation value and standard deviation for the fiber orientation variability s^{f} of $\mathcal{E}(s^{\mathrm{f}}) = 0.3$ and $\mathcal{S}(s^{\mathrm{f}}) = 0.05$. Hence, the material state in the flow range is considered (Seelig et al. [3], Garesci and Fliegener [4]). For the local fiber volume fraction ρ^{f}, the expectation value and standard deviation for the reference case are assumed to be $\mathcal{E}(\rho^{\mathrm{f}}) = 0.15$ and $\mathcal{S}(\rho^{\mathrm{f}}) = 0.03$, respectively, which can be considered as typical properties for standard long fiber reinforced thermoplastic materials. For both random variables, the probability density functions are assumed to be of the logarithmic normal type (9) with the parameters s and μ according to Eq. (10) and the prescribed expectation values and standard deviations.

For the stochastic analysis, the space of the random variables is discretized into a total of 43×64 elements, using with a fine approximation in the range of the expectation values of the respective random variables. With increasing distance to the expectation values, the discretization is coarsened. Ranges in the space of the random variables s^{f} and ρ^{f} which are not relevant for the subsequent computations are left undiscretized for reasons of numerical efficiency.

For all 2752 nodes in the discretized space of the random variables, the effective elastic properties $\bar{E}_k(s_i^{\mathrm{f}}, \rho_j^{\mathrm{f}})$, $\bar{G}_{kl}(s_i^{\mathrm{f}}, \rho_j^{\mathrm{f}})$ and $\bar{\nu}_{kl}(s_i^{\mathrm{f}}, \rho_j^{\mathrm{f}})$ are computed, forming the raw data base for the subsequent probabilistic evaluation. Notice that even for multiple stochastic evaluations, e.g. for parametric studies on the effect of the expectation value and the standard deviation or other variations in the probability distributions for the random variables, both, the computation of the raw data base and the re-arrangement of its contents into ascending order need to be performed only once. Since the probabilistic analysis defined in Sec. 2.2 requires only the computation of the individual probability densities $\Delta\mathcal{F}_{ij}$ according to Eq. (13) and the computation of the cumulative probabilities $\mathcal{F}$ for the effective elastic properties according to Eq. (14) and since both equations define simple multiplication and summation of a limited number of terms, the numerical scheme proves to be rather efficient.

In a first parametric study, the effect of variations in the expectation value $\mathcal{E}(s^{\mathrm{f}})$ of the fiber orientation distribution is analyzed. The expectation value $\mathcal{E}(s^{\mathrm{f}})$ is varied in five steps over the interval $[0.1, 0.5]$ whereas all other quantities defining the uncertainty of the random variables s^{f} and ρ^{f} are kept constant at their basic values as mentioned above. This analysis conforms to the consideration of fife different levels of morphological disorder, e.g. different positions within a component (Seelig et al. [3], Phelps et al. [11]), where the real amount of local morphological disorder is subject to uncertainty. The results in terms of the (cumulative) probability

distributions $\mathcal{F}(\bar{E}_k^{\mathrm{LFT}})$, $\mathcal{F}(\bar{G}_{kl}^{\mathrm{LFT}})$ and $\mathcal{F}(\bar{\nu}_{kl}^{\mathrm{LFT}})$ for the effective Young's and shear moduli as well as for the effective Poisson's ratio are presented in Fig. 7.

For the effective Young's moduli $\bar{E}_k^{\mathrm{LFT}}$ of the long fiber reinforced material, strong effects are observed for the elastic modulus $\bar{E}_1^{\mathrm{LFT}}$ within the flow (or preferred) direction whereas the stiffness of the material perpendicular to this direction remains approximately unaffected. This discrepancy between the effects on the different elastic moduli is due to the different dependence of the individual effective Young's moduli $\bar{E}_k^{\mathrm{LFT}}$ on the random variable s^{f} (see Fig. 6). Since in the relevant range of smaller fiber orientation variabilities, $\bar{E}_2^{\mathrm{LFT}}$ and $\bar{E}_3^{\mathrm{LFT}}$ feature only minor variations with varying fiber orientation variability, uncertainties in the fiber orientation variability s^{f} do not cause significant uncertainties in the effective elastic moduli. All uncertainties on these two effective moduli visible in Fig. 7 are caused by uncertainties in the local fiber volume fraction ρ^{f}. For the effective Young's modulus $\bar{E}_k^{\mathrm{LFT}}$ within the flow direction, a strong dependence on the fiber orientation variability ρ^{f} is observed in Fig. 6. As a consequence, a large amount of the uncertainty in this effective property is caused by the uncertainty in the local fiber orientation variability. Hence, variations in the expectation value $\mathcal{E}(s^{\mathrm{f}})$ cause strong effects on the probability distribution $\mathcal{F}(\bar{E}_1^{\mathrm{LFT}})$. Increasing expectation values $\mathcal{E}(s^{\mathrm{f}})$ result in decreasing effective elastic moduli $\bar{E}_1^{\mathrm{LFT}}$. Due to the nonlinear dependence of the raw data base on the random variable s^{f}, variations in the expectation value $\mathcal{E}(s^{\mathrm{f}})$ at constant standard deviation $\mathcal{S}(s^{\mathrm{f}})$ (and thus a constant scatter band width) of the input property s^{f} do not only affect position of the scatter band of the output property $\bar{E}_1^{\mathrm{LFT}}$ (e.g. characterized by its median value), but also has distinct effects on the scatter band width.

For the effective shear moduli $\bar{G}_{23}^{\mathrm{LFT}}$, $\bar{G}_{13}^{\mathrm{LFT}}$ and $\bar{G}_{12}^{\mathrm{LFT}}$, qualitatively similar – although quantitatively less distinct – effects are observed. The effective transverse shear moduli $\bar{G}_{23}^{\mathrm{LFT}}$ and $\bar{G}_{13}^{\mathrm{LFT}}$, which show only a rather weak dependence on the random variable s^{f} (see Fig. 6) are nearly unaffected by variations in its expectation value $\mathcal{E}(s^{\mathrm{f}})$. For the in-plane shear modulus $\bar{G}_{12}^{\mathrm{LFT}}$, it is observed that for increasing expectation values $\mathcal{E}(s^{\mathrm{f}})$, the probability distributions $\mathcal{F}(\bar{G}_{12}^{\mathrm{LFT}})$ are shifted towards higher values. In contrast to the effective Young's modulus $\bar{E}_1^{\mathrm{LFT}}$, the shape of the probability distributions $\mathcal{F}(\bar{G}_{12}^{\mathrm{LFT}})$ does not change significantly with increasing expectation value $\mathcal{E}(s^{\mathrm{f}})$, since the variations of the effective shear moduli $\bar{G}_{12}^{\mathrm{LFT}}$ with the random variable s^{f} are less distinct. Similar effects are observed for the effective Poisson's ratios $\bar{\nu}_{32}^{\mathrm{LFT}}$, $\bar{\nu}_{31}^{\mathrm{LFT}}$ and $\bar{\nu}_{21}^{\mathrm{LFT}}$. For all three effective Poisson's ratios, non-negligible effects of the fiber orientation variability s^{f} are observed in Fig. 6. As a consequence, distinct effects of the expectation value $\mathcal{E}(s^{\mathrm{f}})$ on the probability distributions $\mathcal{F}(\bar{\nu}_{ij}^{\mathrm{LFT}})$ for all three effective Poisson's ratios are observed. The most distinct effects are obtained in case of $\bar{\nu}_{21}^{\mathrm{LFT}}$ featuring the strongest dependence on the random variable s^{f} in the relevant range of the random variable hyper space (see Fig 6). Depending on the type of the dependence of the respective effective material property $\bar{E}_i^{\mathrm{LFT}}$, $\bar{G}_{ij}^{\mathrm{LFT}}$ or $\bar{\nu}_{ij}^{\mathrm{LFT}}$ on the random variables s^{f} and ρ^{f} distinctively asymmetric probability distributions $\mathcal{F}(\bar{E}_i^{\mathrm{LFT}})$, $\mathcal{F}(\bar{G}_{ij}^{\mathrm{LFT}})$ or $\mathcal{F}(\bar{\nu}_{ij}^{\mathrm{LFT}})$, respectively, with a non-negligible skewness may develop.

In a second parametric study, the effect of the scatter band width of the fiber orientation variability in terms of its standard deviation $\mathcal{S}(s^{\mathrm{f}})$ on the uncertainty of the effective material parameters $\bar{E}_i^{\mathrm{LFT}}$, $\bar{G}_{ij}^{\mathrm{LFT}}$ and $\bar{\nu}_{ij}^{\mathrm{LFT}}$ is analyzed. The results for their probability distributions are presented in Fig. 8. In this context, only the standard deviation $\mathcal{S}(s^{\mathrm{f}})$ is varied in five steps over the intervall $[0.02, 0.1]$ whereas all other prescribed stochastic descriptors are kept constant at their basic values as mentioned above. This analysis conforms to the consideration of a specific spatial position within the microstructure, featuring a prescribed mean disorder of the fiber orientation (Seelig et al. [3], Phelps et al. [11], Lusti et al. [14]) with different scatter band widths.

In a similar manner as in the parametric study on the effect of the expectation value $\mathcal{E}(s^{\mathrm{f}})$ of the fiber orientation variability in Fig. 7, significant effects of its standard deviation $\mathcal{S}(s^{\mathrm{f}})$ are observed only in those effective elastic properties, which feature a distinct dependence on the random variable s^{f}, i.e. the elastic modulus $\bar{E}_1^{\mathrm{LFT}}$ within the flow direction, the in-plane shear modulus $\bar{G}_{12}^{\mathrm{LFT}}$, the in-plane Poisson's ratio $\bar{\nu}_{12}^{\mathrm{LFT}}$ and – although less distinct – the transverse Poisson's ratios $\bar{\nu}_{13}^{\mathrm{LFT}}$ and $\bar{\nu}_{23}^{\mathrm{LFT}}$. As expected, increasing scatter band widths of the effective elastic properties are obtained with increasing scatter band width of the random variable in terms of its standard deviation $\mathcal{S}(s^{\mathrm{f}})$. The predicted scatter band width is well within the range of the experimental investigation by Thomason [21] on the effects of the microstructure of injection molded long glass fiber reinforced polyamide 6.6 materials on their effective properties. In this study, an uncertainty range for the effective Young's modulus defined as twice the standard deviation in the range of up to $10, ...15\%$ of the mean elastic modulus is reported.

Although this is a minor effect in the present example, it is observed that the standard deviation and thus the scatter band width of the random variable does not only affect the shape (or spreading) of the probability distributions $\mathcal{F}$ of the elastic properties but also may have effects on their position. This effect is visible through a shift of the common point of all probability distributions for a specific effective property from the median probability $\mathcal{F} = 0.5$. In the present example, this point is shifted below the median in the case of $\bar{E}_1^{\mathrm{LFT}}$ and

beyond the median for the in-pane Poisson's ratio $\bar{\nu}_{21}^{\mathrm{LFT}}$. More distinct effects of this type will be observed in the final parametric study (Fig. 10).

In two final parametric studies, the effect of the expectation value $\mathcal{E}(\rho^{\mathrm{f}})$ and the standard deviation $\mathcal{S}(\rho^{\mathrm{f}})$ of the local fiber volume fraction ρ^{f} are studied. The results are compiled in Figs. 9 and 10 respectively. In contrast to the two previous parametric studies on the effect of the expectation value and the uncertainty of the fiber orientation variability, the uncertainty descriptors $\mathcal{E}(\rho^{\mathrm{f}})$ and $\mathcal{S}(\rho^{\mathrm{f}})$ are found to affect the probability distributions and thus the uncertainty for all effective elastic properties. This effect is caused by the fact that the local fiber volume fraction ρ^{f} – in contrast to the (in-plane) fiber orientation variability s^{f} – affects all effective elastic constants (see Fig. 6). Hence, variabilities in this random variable essentially result in uncertainties in the macroscopic material property values based thereon. As before, the strength of the effect of the microstructural uncertainty on the material uncertainty on the macroscopic level depends on the type and order of the dependence of the raw data base on the respective random variable.

4 Conclusions

The objective of the present study has been a numerical procedure for the prediction of the uncertainty and scatter to be expected in the effective elastic constants of long fiber reinforced thermoplastic (LFT) materials caused by the geometric uncertainty in the microstucture. The geometrc uncertainty of the microstructure is assumed to be governed by uncertainties in the local fiber density as wellas in the local fiber orientation distribution as the two features mainly controlling the effective stiffness of the material. For the probabilistic analysis, a numerical scheme has been adopted, which is based on prescribed discretization of the space of the random variables and a determination of the individual probabilities for the occurrence of the discrete values of the random variables rather than on a direct Monte-Carlo analysis.

The proposed discretizing scheme proves to be numerically stable and rather efficient. In this context, it should be noticed that all of the results figures contain direct numerical data without any smoothing. Despite the large number of elements in the discretization of the random variable space – which has been used here in order to enable parametric studies over a wide range of material parameters – only 20 to 30 data are typically in the active range, i.e. in the range of the increase of the probability distributions. Their vast majority is found in the upper and lower tails. Hence, by an appropriate choice of the discretization of the space of the random variables, rather efficient analyses are possible by the proposed scheme.

In the application of the proposed numerical method to the example of a long glass fiber reinforced polyamide 6 composite, it is observed that the microscopic morphological uncertainties may cause distinct material uncertainties on the macroscopic level. The individual effective elastic properties of the material are affected by the morphological uncertainties in a different manner, dependent on the respective microscopic mechanism of deformation. The resulting probability distributions are of an essentially non-Gaussian type. In this context, it is observed that the scatter of the random variables defining the microstructure does not only affect the scatter band widths of the effective elastic constants on the macroscale but might also affect their median or mean values respectively. The results reveal again that a proper stochastic analysis is essential for a comprehensive assessment of the material uncertainties. Since the molding process controls the local fiber orientation distribution, the molding process must be considered contemporarily to the geometric design of the structure. The output of the present probabilistic assessment of the effective elastic constants may form the input for a stochastic finite element analysis on the structural level, providing the uncertainty to be expected in the response of LFT components under service loads or accidental conditions. A proper stochastic assessment of the structural response during the design process enables an improved prediction of the structural behaviour accounting for all kinds of uncertainties and thus might enable the reduction of unnecessarily large safty factors. Other future topics include the extension of the present approach to the effective properties in the nonlinear range such as the plastic material response as well as the effects of damage and failure. By this means the effective strength will be included in order to be able to assess the scatter to be expected in the load carrying capacity of LFT structures.

Acknowledgement

The present work has been funded by the Deutsche Forschungsgemeinschaft (DFG, German Research Foundation) under grant no. Ho 1852/6-2. The financial support is gratefully acknowledged.

References

[1] Skourlis, T.P., Pochiraju, K., Chassapis, C. and Manoocheri, S.: Structure-modulus relationships for injection-molded long fiber-reinforced polyphtalamides, Compos. B **29** (1998) 309-320.

[2] Teixeira, D., Giovanela, M., Gonella, L.B. and Crespo, J.S.: *Influence of flow restriction on the microstructure and mechanical properties of long glass fiber-reinforced polyamide 6.6 composites for automotive applications*, Mat. Des. **47** (2013) 287-294.

[3] Seelig, T., Latz, A. and Sanwald, S.: Modelling and crash simulation of long-fibre-reinforced thermoplastics, Proc. 7^{th} LS-DYNA User's Conference (Bamberg, 2008), D-I-33–D-I-40.

[4] Garesci, F. and Fliegener, S.: Young's modulus prediction of long fiber reinforced thermoplastics, Compos. Sci. Tech. **85** (2013) 142-147.

[5] Thomason, J.L.: The influence of fibre length and concentration on the properties of glass fibre reinforced polypropylene. 6: The properties of injection moulded long fibre PP at high fibre content, Compos. A **36** (2005) 995-1003.

[6] Taya, M. and Chou, T.W.: Prediction of the stress-strain curve of a short-fiber reinforced thermoplastic, J. Mat. Sci. **17** (1982) 2801-2808.

[7] Nguyen, B.N. and Khaleel, M.A.: A mechanistic approach to damage in short-fiber composites based on micromechanical and continuum damage mechanics descriptions, Compos. Sci. Tech. **64** (2004) 607-617.

[8] Dunn, M.L., Ledbetter, H., Heylinger, P.R. and Choi, C.S.: Elastic constants of textured short-fiber composites, J. Mech. Phys. Solids **44** (1996) 1509-1541.

[9] Fu, S.Y. and Lauke, B.: Effects of fiber length and fiber orientation distributions on the tensile strength of short-fiber-reinforced polymers, Compos. Sci. Tech. **56** (1996) 1179-1190.

[10] Bijsterbosch, H. and Gaymans, R.J.: Polyamide 6 - long glass fiber injection moldings, Polmer Compos. **16** (1995) 363-369.

[11] Phelps, J.H., Abd El-Rahman, A.I., Kunc, V. and Tucker, C.L.: A model for fiber length attrition in injection-molded long-fiber composites, Compos. A **51** (2013) 11-21.

[12] Sriramula, S. and Chryssanthopoulos, M.K.: Quantification of uncertainty modelling in stochastic analysis of FRP composites, Compos. A **40** (2009) 1673-1684.

[13] Mesogitis, T.S., Skordos, A.A. and Long, A.C.: Uncertainty in the manufacturing of fibrous thermosetting composites: A review, Compos. A **57** (2014) 67-75.

[14] Lusti, H.R., Hine, P.J. and Gusev, A.A.: Direct numerical predictions for the elastic and thermoelastic properties of short fiber composites, Compos. Sci. Tech. **62** (2002) 1927-1934.

[15] Lee, Y. and Jasiuk, I.: Apparent elastic properties of random fiber networks, Comput. Mat. Sci. **79** (2013) 715-723.

[16] Dirrenberger, J., Forest, S. and Jeulin, D.: Towards gigantic RVE sizes for 3D stochastic fibrous networks, Int. J. Solids Struct. **51** (2014) 359-376.

[17] Rahman, S. and Chakraborty, A.: A stochastic micromechanical model for elastic properties of functionally graded materials, Mech. Mat. **39** (2007) 548-563.

[18] Soize, C.: Non-Gaussian positive-definite matrix-valued random fields for elliptic stochastic partial differential operators, Comput. Meth. Appl. Mech. Eng. **195** (2006) 26-64.

[19] Hohe, J., Hardenacke, V.: Analysis of uncertainty effects due to microstructural disorder in cellular or porous materials, Int. J. Solids Struct. **49** (2012) 1009-1921.

[20] Beckmann, C. and Hohe, J.: Assessment of material uncertainties in solid foams based on local homogenization procedures, Int. J. Solids Struct. **49** (2012) 2807-2822.

[21] Thomason, J.L.: The influence of fibre length, diameter and concentration on the modulus of glass fibre reinforced polyamide 6.6, Compos. A **39** (2008) 1732-1738.

List of Figures

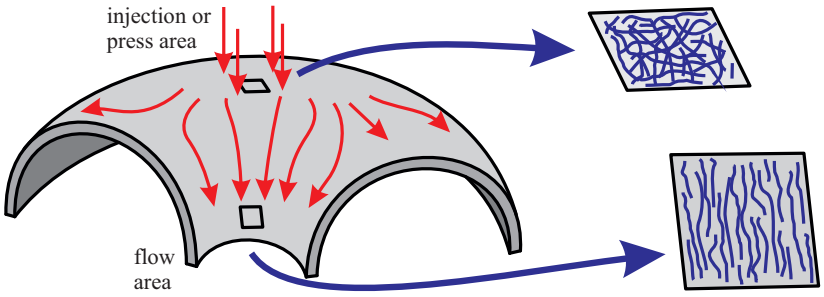

Figure 1: Fiber orientation in structures consisting of long fiber reinforced materials.

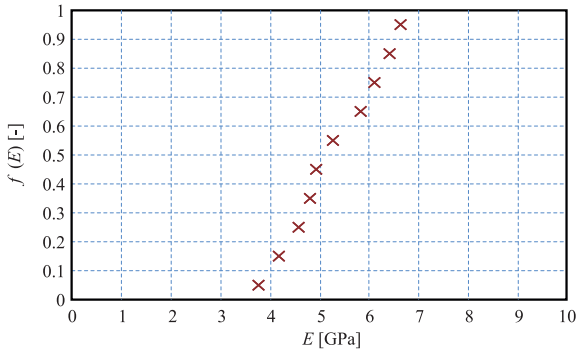

Figure 2: Probability distribution of the secant modulus for LFT material (data by Seelig et al. [3]).

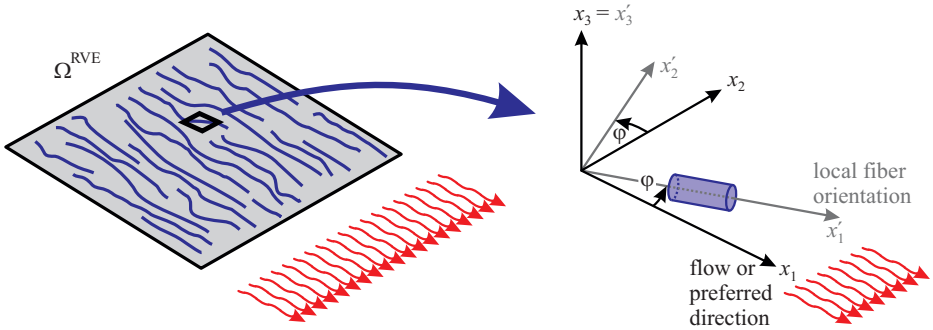

Figure 3: Coordinate systems.

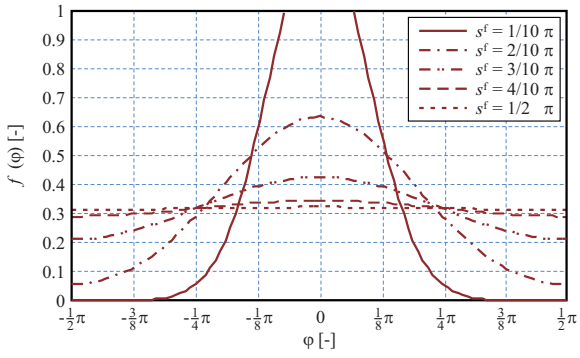

Figure 4: Probability density distribution for fiber orientation.

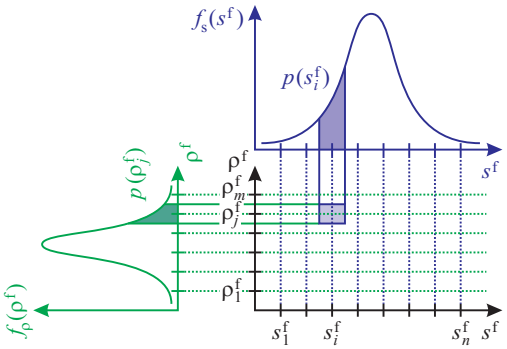

Figure 5: Discretization of the space of the random variables.

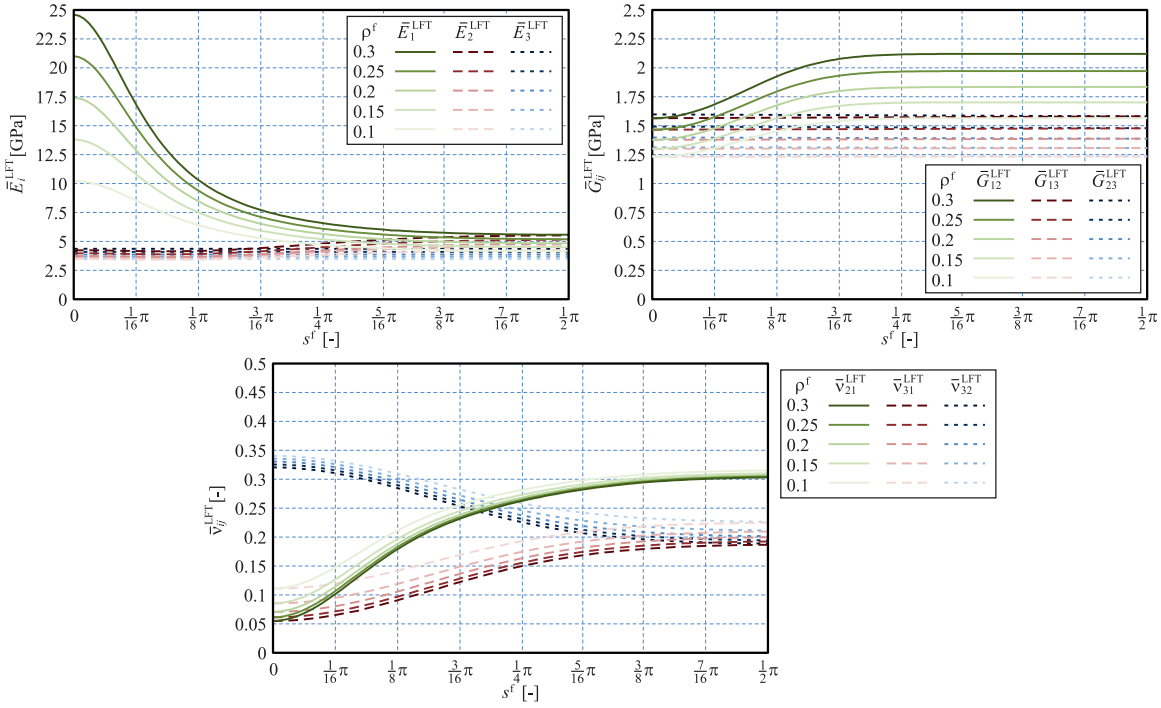

Figure 6: Dependence of the elasticity parameters on the stochastic variables.

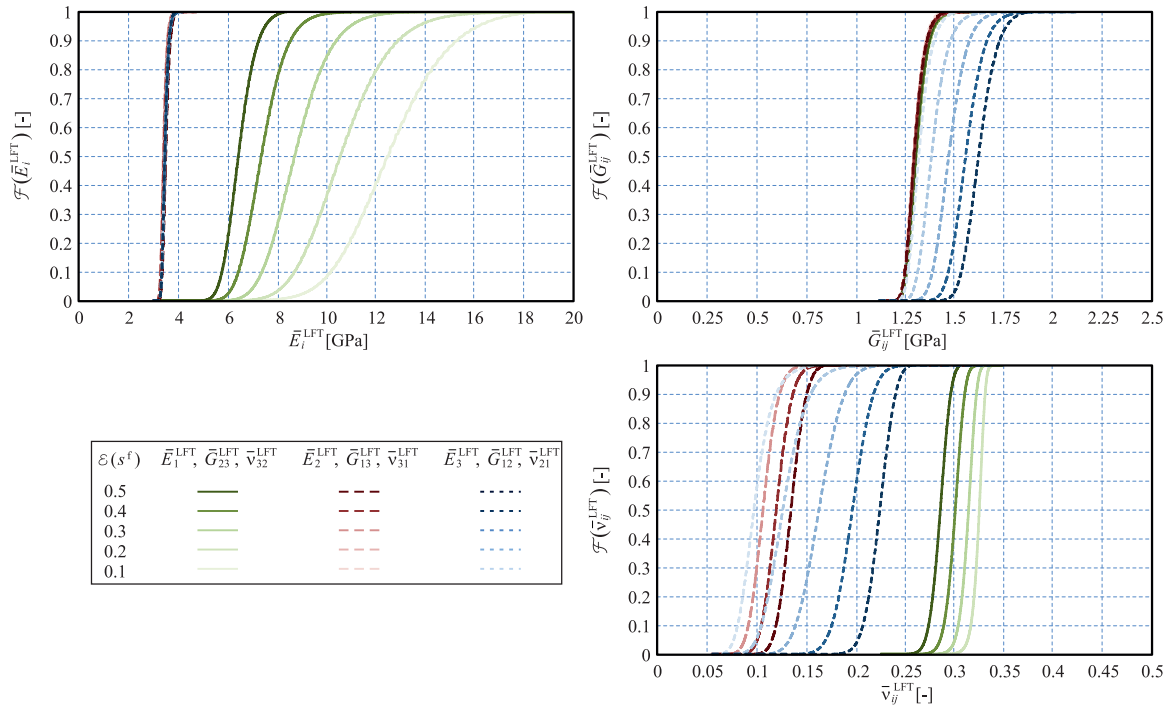

Figure 7: Probabilistic analysis - variation of the expectation value for the fiber orientation variability s^{f}.

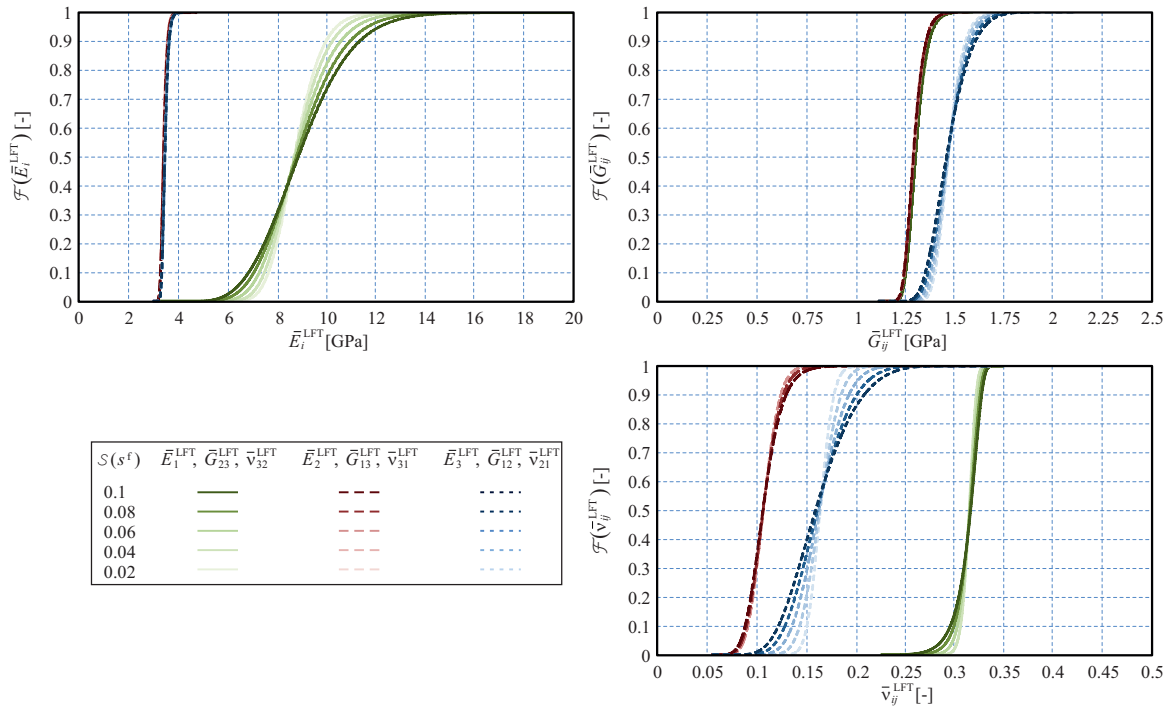

Figure 8: Probabilistic analysis - variation of the standard deviation for the fiber orientation variability s^{f}.

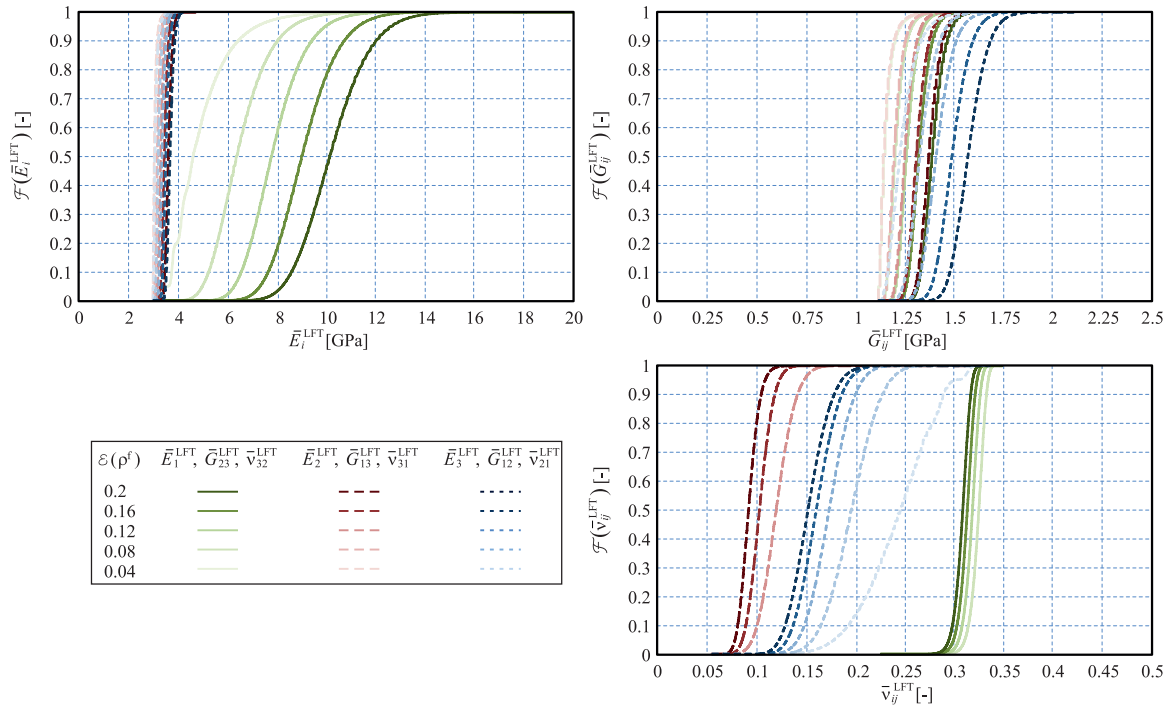

Figure 9: Probabilistic analysis - variation of the expectation value for the local fiber volume fraction ρ^{f}.

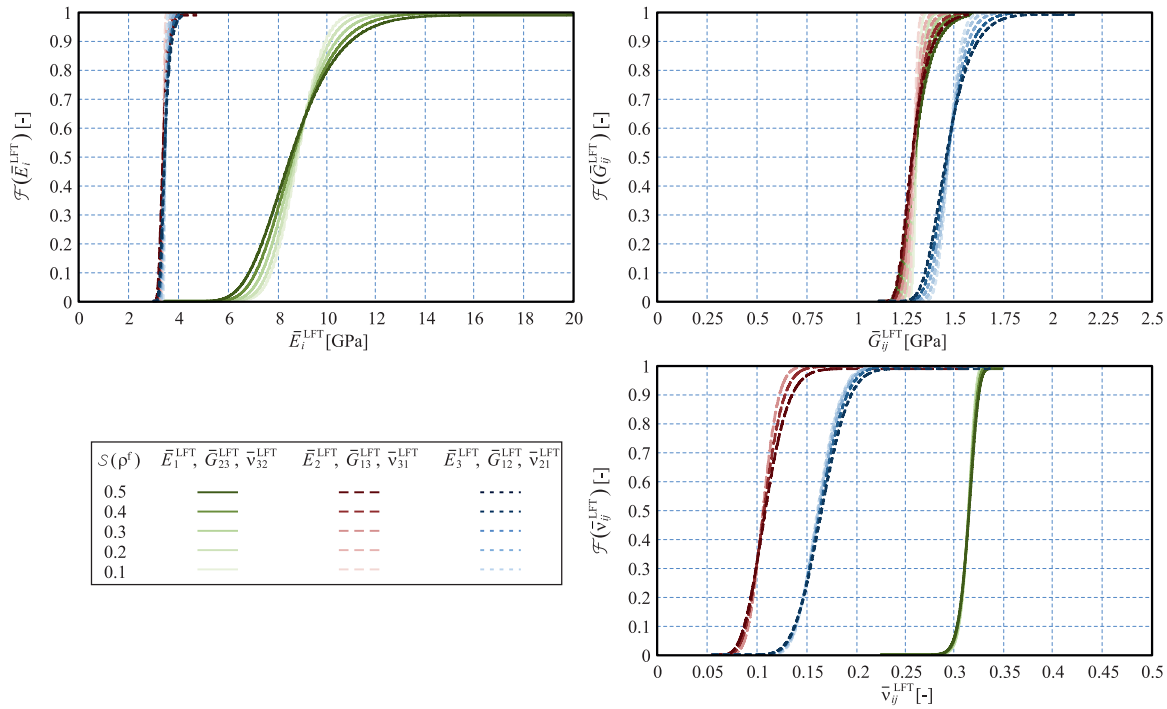

Figure 10: Probabilistic analysis - variation of the standard deviation for the local fiber volume fraction ρ^{f}.